# Volume and Compressibility Differences Between Protein Conformations Revealed by High-Pressure NMR

1 Xingjian  $Xu^{1,2}$ , Donald Gagné<sup>1,†</sup>, James M. Aramini<sup>1</sup>, Kevin H. Gardner<sup>1,3,4,\*</sup> 2 3 <sup>1</sup>Structural Biology Initiative, CUNY Advanced Science Research Center, New York, NY, USA 4 <sup>2</sup>Ph.D Program in Biochemistry, The Graduate Center, CUNY, New York, NY, USA 5 <sup>3</sup>Department of Chemistry and Biochemistry, City College of New York, New York, NY, USA 6 7 <sup>4</sup>Ph.D. Programs in Biochemistry, Chemistry, and Biology, The Graduate Center, CUNY, New York, NY, USA 8 †: current address: Kisoji Biotechnology, Montréal, QC, Canada 9 \*: address correspondence to: 10 11 Kevin Gardner, Structural Biology Initiative, CUNY Advanced Science Research Center, 85 St. Nicholas Terrace, New York, NY 10031 USA, E-mail: kgardner@gc.cuny.edu; phone: +1 12 212 413 3220 13 14 15

#### **ABSTRACT**

Proteins often interconvert between different conformations in ways critical to their function. While manipulating such equilibria for biophysical study is often challenging, the application of pressure is a potential route to achieve such control by favoring the population of lower volume states. Here, we use this feature to study the interconversion of ARNT PAS-B Y456T, which undergoes a dramatic +3 slip in beta-strand register as it switches between two stably-folded conformations. Using high pressure biomolecular NMR approaches, we obtained the first quantitative data testing two key hypotheses of this process: the slipped conformation is both smaller and less compressible than the wildtype equivalent, and the interconversion proceeds through a chiefly-unfolded intermediate state. Data collected in steady state pressure and time-resolved pressure-jump modes, including observed pressure-dependent changes in the populations of the two conformers and increased rate of interconversion between conformers, support both hypotheses. Our work exemplifies how these approaches, which can be generally applied to protein conformational switches, can provide unique information that is not easily accessible through other techniques.

#### STATEMENT OF SIGNIFICANCE

Proteins often interconvert between conformations via processes that can be difficult to characterize due to the low populations and short lifetimes of intermediate and end states. This can be addressed with high-pressure perturbation stabilizing conformations with smaller system volumes, as elegantly applied in high pressure NMR studies of protein folding. Here we demonstrate comparable utility for probing the thermodynamics and kinetics of a protein interconverting between two stably-folded conformations. Combining steady-state and time-resolved pressure NMR, we measured volumes and compressibilities of ground and intermediate states which are otherwise challenging to access, letting us test a proposed interconversion mechanism. These data establish both fundamental parameters of the process and guide artificial control via ligand binding.

#### INTRODUCTION

The energy landscape theory of folding states that proteins sample many conformations before reaching the native state (1, 2). Although the native conformation is usually the lowest free energy state under physiological conditions, proteins can be trapped in stably-folded local minima that are markedly different from the native conformation (3-5). Transitions between conformations, which can be spontaneous or triggered by changes in environmental conditions (e.g. pH, temperature, light) or ligand binding, are often critical for shifting proteins between functionally inactive and active forms (3-7). Such shifts can range from simple local rearrangements to 'metamorphic' proteins, which reversibly adopt different stable folds in different environmental conditions (8-10). However, identifying and characterizing alternative conformational states of proteins can be challenging, as they are often high-energy states and sparsely populated (11, 12). Several techniques currently allow quantitative characterization of conformational sub-states despite challenges introduced by low population, particularly solution nuclear magnetic resonance (NMR) techniques such as relaxation dispersion experiments (11-14).

To aid in characterizing such excited states, it is routine for one to manipulate their populations by adding small molecule ligands or changing experimental conditions, such as pH or temperature (11, 15-17). Increasingly, pressure has also been utilized to control conformational equilibria, aided by the introduction of commercially-built pumps and sample cells compatible with NMR and other biophysical instrumentation (18-20). Pressure directly affects such equilibria by acting on differences in the partial volumes and compressibilities of different conformers, with increasing pressure favoring those with lower volumes (21). Given that unfolded proteins are generally smaller than their folded forms, pressure studies have been

particularly useful at investigating protein unfolding reactions, which typically occur above 2000 bar under native conditions (20-25). However, the application of sub-unfolding pressures can cause proteins to shift populations among multiple folded states (18, 26-28), providing an easy way to manipulate protein conformational equilibria to facilitate their study.

These advantages of pressure-NMR led us to examine its applicability to characterize a protein domain which slowly exchanges between two folded states via an unusual  $\beta$ -strand slip (29, 30). This system is derived from the human ARNT (Aryl hydrocarbon Receptor Nuclear Translocator) protein, a bHLH-PAS (basic helix-loop-helix / Per-ARNT-Sim) transcription factor which binds a variety of partners via its two PAS domains, PAS-A and PAS-B (31-35). PAS domains adopt a mixed  $\alpha/\beta$  fold, with helical and sheet layers often encapsulating internal cavities between them (31, 32, 34). In many cases, these internal cavities provide binding sites for natural or artificial regulatory molecules (36). For ARNT PAS-B, 105 Å<sup>3</sup> of interconnected internal cavities are seen in the crystal structure, suggesting that small molecules may bind there and control the role of ARNT in several signaling pathways (29, 32, 37, 38).

We have previously reported that the ARNT PAS-B  $\beta$ -sheet can surprisingly adopt an alternatively-folded conformation in certain settings. For example, a Y456T point mutation at a site preceding the final  $\beta$ -strand enables the domain to adopt a new conformation that coexists in a 1:1 equilibrium with the WT fold at room temperature (29, 30) (**Fig. 1**). Additional mutations to nearby residues (F444Q/F446A/Y456T, hereafter called the TRIP variant) stabilized this alternative conformation, letting us characterize the new structure and show that it differs from the WT conformation by a three residue slip of central I $\beta$ -strand of the domain's five-stranded  $\beta$ -sheet. This slip inverts the topology of the I $\beta$ -strand and isomerizes the neighboring N448-P449

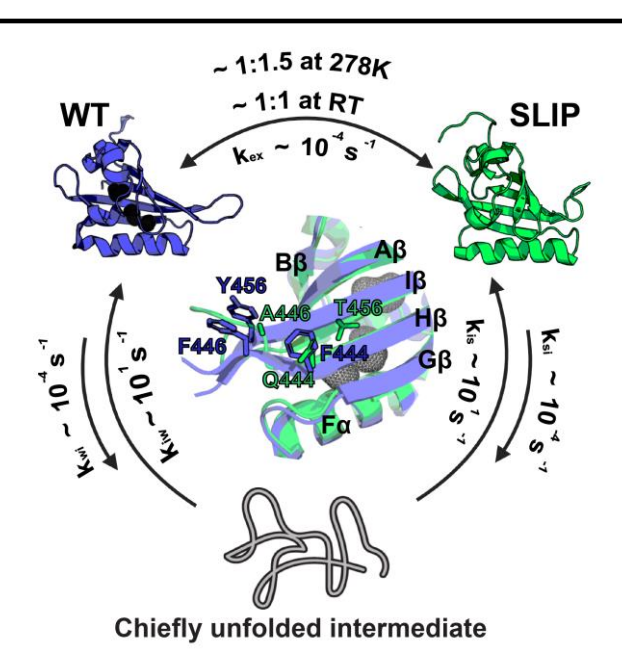


**Figure 1. Current model of ARNT PAS-B Y456T interconversion between the WT and SLIP conformation.** Prior work demonstrated that this protein interconverts between the folded WT and SLIP conformations on the same timescale as the unfolding rates of either conformer, implying a slow transition process requiring a chiefly unfolded intermediate state. The two conformations are in 1:1 equilibrium at room temperature, but lower temperature favors the SLIP conformation (1:1.5 at 278K). The F444Q/F446A/Y456T variant (TRIP) locks the protein in the SLIP conformation, structural comparison between WT (blue) and TRIP (green) is displayed in the middle, with mutation sites labeled.

peptide bond, collectively abolishing the domain's ability to interact with some other binding partners (29). Notably, the threonine side chain introduced by the Y456T mutation fills an internal cavity (29, 30), leading us to suspect that interconversion process could be manipulated by pressure perturbations (18, 39-42) to obtain thermodynamic and kinetic information complementary to our prior structural studies.

Here we report results from high-pressure solution NMR studies of ARNT PAS-B Y456T, letting us for the first time obtain quantitative measurements of several thermodynamic and kinetic parameters of the WT:SLIP interconversion. We found that the WT conformation is not only larger in volume than SLIP, but also more compressible as perhaps due to the cavities unique to the WT conformation (29, 32). Additionally, we tested a hypothesis that WT:SLIP interconversion proceeds through a chiefly unfolded intermediate state, previously suggested

from the similarities of interconversion and unfolding rates (30). We found that pressure increases the rate of interconversion, letting us measure both the activation volume and compressibility (30), both validating this model and allowing us to quantitate how unfolded the transition state is. Finally, we demonstrated that both residue-specific compressibility and pressure-dependent chemical shift changes can predict whether residues are near cavities, providing insights into locations of such cavities within the protein. Taken together, our approach exemplifies the ability of high-pressure NMR to enable thermodynamic and kinetic analyses of protein conformational transitions that are otherwise inaccessible.

#### MATERIALS AND METHODS

#### **Protein Purification and Expression**

His6-tagged human ARNT PAS-B (residues 356-470) WT and mutants (Y456T and F444Q/F446A/Y456T) were uniformly labeled with <sup>13</sup>C and <sup>15</sup>N and overexpressed in BL21 (DE3) E. coli. Isotopically-labeled proteins were obtained by growing cells in M9 media supplemented with 3 g/L U-<sup>13</sup>C6 glucose and 1 g/L <sup>15</sup>NH4Cl as the carbon and nitrogen sources, respectively. Cells were incubated at 37 °C until an OD600 of 0.6-0.8. Protein expression was induced with 0.5 mM Isopropyl-β-D-thiogalactopyranoside (IPTG) and incubated overnight (~ 16-18 hr) at 18 °C. Cells were harvested next day, cell pellets were resuspended in 50 mM Tris (pH 7.5), 150 mM NaCl, 10 mM imidazole, 1 mM DTT buffer containing 1 mM PMSF, lysed with sonication, and centrifuged. Supernatant was incubated with 5 mL of Ni<sup>2+</sup> Sepharose<sup>TM</sup> High Performance beads and eluted with 500 mM imidazole buffer. His6-Tagged ARNT PAS-B proteins were exchanged into a low imidazole buffer (8 mM imidazole, 50 mM Tris (pH 7.5), 150 mM NaCl, and 1 mM DTT) and incubated overnight with His6-tobacco etch virus (TEV) protease for tag cleavage. The freed His6-tag and His6-TEV were removed by a second round of

 $Ni^{2+}$  column purification. ARNT PAS-B proteins were further purified by passing through a Superdex 75 size exclusion column and exchanged into baroresistant buffer (44.7 mM Tris pH 7.0, 5.3 mM phosphate, 17 mM NaCl, 1 mM DTT) (43) and concentrated with an Amicon stirred ultrafiltration unit with a 3 kDa filter to 320  $\mu$ M. Samples were flash frozen with liquid nitrogen and were stored at -80 °C for later use.

#### **Pressure-Jump NMR Experiments**

122

123

124

125

126

127

128

129

130

131

132

133

134

135

136

137

138

139

140

141

142

143

144

Solution NMR experiments were performed on a Bruker Avance III HD 700 MHz NMR spectrometer equipped with a 5-mm QCI-F cryoprobe. NMR samples were prepared by mixing 80% of the purified protein samples with 20% D<sub>2</sub>O yielding a final concentration of around 250 uM. Samples were loaded into a commercially-available pressure resistant NMR cell (Daedalus Innovations, Aston, PA, USA), with pressure between 20 bar to 2500 bar applied through a Xtreme-60 Syringe Pump from the same vendor. The baseline pressure was set to 20 bar as it is a low pressure that can be stably maintained by the pump. We performed two types of pressurejump experiments, direct pressure-jump experiments where pressure was increased directly from 20 bar to the destination pressure of up to 2500 bar, and cumulative step pressure-jump experiments with constant intervals, where pressure was increased incrementally from baseline pressure to the final pressure of 2500 bar. To set up direct pressure-jump experiments, samples were thawed and stored on ice, and first equilibrated at 20 bar and 278.1 K for 1 hr and raised to a higher pressure (between 125 bar to 1500 bar) and equilibrated at that pressure. As identified in preliminary experiments, the duration of equilibration process varies depending on the pressure: interconversion of the two populations at 20 bar takes around 12 hours to complete, while it occurs more quickly as pressure increases (30). Equilibration time under pressure was therefore set to 12 hr at 125 bar, and gradually reduced to 5 hr for pressures between 500 to 1000 bar, and

finally 4 hr for pressures beyond 1000 bar. During the equilibration, a series of 1D <sup>13</sup>C edited <sup>1</sup>H NMR experiments were recorded to detect the rate of interconversion, with each spectrum requiring ca. 4.25 min to acquire. The system was relaxed for 12.5 hr at 20 bar post equilibrations at different pressures, 1D <sup>13</sup>C-edited <sup>1</sup>H NMR experiments were also recorded during relaxation. For step pressure-jump experiments, samples were first equilibrated at 20 bar and 278.1K, then pressurized and equilibrated in steps of 250 bar, until reaching 2500 bar. Equilibration time was set to 9 hr at 250 bar, 6 hr at 500 bar, 5 hr for 750 and 1000 bar, and 4 hr for 1250, 1500, 1750, 2000, and 2250 bar. Equilibration time was extended to 6 hr at 2500 bar to monitor any unfolding effects at the highest pressure safely accessible with our instrumentation. 1D NMR spectra were acquired as described earlier. <sup>15</sup>N/<sup>1</sup>H and <sup>13</sup>C/<sup>1</sup>H HSQC spectra were also acquired at system equilibrium at 20, 250, 500, 750, 1000, 1250, 1500, and 2500 bar. <sup>15</sup>N/<sup>1</sup>H HSQC experiments were acquired with 16 scans and FIDs of 2048x256 complex points. <sup>13</sup>C/<sup>1</sup>H HSQC experiments were acquired with 8 scans and FID of 2048x256 complex points. All NMR spectra were processed and analyzed with NMRFx Analyst and NMRViewJ (44, 45). Chemical shift assignments from previous NMR assignments of ARNT PAS-B WT and F444Q/F446A/Y456T mutant were used for all analyses (29, 31).

145

146

147

148

149

150

151

152

153

154

155

156

157

158

159

160

161

162

163

164

165

Unfolding measurements of ARNT PAS-B WT and the F444Q/F446A/Y456T variant under pressures accessible by our apparatus (20-2500 bar) was achieved by the addition of urea (up to 3.0 M). <sup>15</sup>N/<sup>1</sup>H HSQC spectra were acquired between 20 and 2500 bar with increments of 250 bar. Peak assignments from previous work were obtained (29, 31), and transferred to the acquired spectra following urea titration experiments between 0.5 and 3.0 M.

#### **NMR Data Analysis**

In the 1D <sup>13</sup>C-edited <sup>1</sup>H NMR experiments, two peaks corresponding to the L391-δ1 methyl group of the WT and SLIP conformations were used to determine the populations of each conformational state of the protein in the sample. The relative populations (SLIP/WT) at different pressures were obtained by taking the ratio of the integrals of the two peaks. The equilibration (change in relative population) under different pressures and the rates of interconversion were obtained by plotting the relative population as a function of time.

The equilibrium constant *K* between the two conformers of the ARNT PAS-B Y456T is given by the relation

$$K = \frac{[SLIP]}{[WT]} = e^{-\Delta G/RT}$$
 (1)

Since the temperature T was kept constant during the pressure jump experiments, the free energy  $\Delta G$  scales only with pressure p. The free energy as a function of pressure can be approximated by a Taylor expansion

179 
$$\Delta G(p) = \Delta G^{0} + \Delta V^{0}(p - p_{0}) - \frac{1}{2} \times \Delta \beta V^{0}(p - p_{0})^{2} + \dots + \frac{\Delta G^{n}(p_{0})}{n!}(p - p_{0})^{n}$$
 (2)

 $\Delta G^0$  is the free energy between the two conformers at ambient pressure,  $\Delta V^0$  is the volume difference between the two conformers, representing the first derivative of free energy with respect to pressure, and compressibility between the two conformations,  $\Delta \beta V^0$ , is the second derivative of free energy, with respect to pressure. The equilibrium constants were plotted as a function of pressure, and fit to the following equation, incorporating up to the third term of the Taylor series (18):

186 
$$K_{eq} = e^{-\left(\Delta G^0 + (p - p_0)\Delta V^0 - 1/2 \times \Delta \beta V^0 (p - p_0)^2\right)/RT}$$
 (3)

187 The pressure was referenced to atmospheric pressure,  $p_0=1$  bar.

The observed rate of increase of one conformation (or decrease of the other conformation) as a function of pressure could be fit to a biexponential equation:

190 
$$k_{obs} = k_{sw0} e^{-\left(p\Delta V_{sw}^{\dagger} - 1/2\Delta\beta V_{sw}^{\dagger} p^{2}\right)/RT} + k_{ws0} e^{-\left(p\Delta V_{ws}^{\dagger} - 1/2\Delta\beta V_{ws}^{\dagger} p^{2}\right)/RT}$$
(4)

yielding the activation volumes ( $\Delta V_{sw}^{\ddagger}$  and  $\Delta V_{ws}^{\ddagger}$ ) and compressibility differences between the two folded conformations (WT and SLIP) to the previously-proposed, chiefly unfolded intermediate state ( $\Delta\beta V_{sw}^{\ddagger}$  and  $\Delta\beta V_{ws}^{\ddagger}$ ) (30). Together with the two initial rate constants at ambient pressure ( $k_{sw0}$ , SLIP to WT, and  $k_{ws0}$ , WT to SLIP), there were 6 unknown parameters to be fit. To better approximate the two exponential terms, rates at different pressures were solved numerically using the following differential equation pair:

$$\frac{d[S]}{dt} = -k_{sw}[S] + k_{ws}[W] \quad (5)$$

$$\frac{d[W]}{dt} = k_{sw}[S] - k_{ws}[W]$$
 (6)

The fittings were done in R, using the package deSolve as the ordinary differential equation solver, and Levenberg-Marquardt Nonlinear Least-Squares Algorithm in minpack.lm for parameter fitting (46). The uncertainty of the fitting was estimated by calculating the 95% confidence intervals from the variance covariance matrix of the fit rate constants. 95% confidence intervals were further verified with a bootstrapping procedure. Random noises with mean of 0 and variance of the mean square error from the model were added to the raw data and

fit repeatedly. The estimated parameters were computed to determine if they fall within the 95% confidence interval. The rates of interconversion at any given pressure ( $k_{sw}$  for SLIP to WT,  $k_{ws}$  for WT to SLIP) were plotted separately as functions of pressure, and fit individually to:

$$k_{sw} = k_{sw0} e^{-\left(p\Delta V_{sw}^{\dagger} - 1/2\Delta\beta V_{sw}^{\dagger} p^2\right)/RT}$$
 (7)

$$k_{ws} = k_{ws0} e^{-(p\Delta V_{ws}^* - 1/2\Delta\beta V_{ws}^* p^2)/RT}$$
 (8)

obtaining rates at ambient pressure ( $k_{sw0}$ ,  $k_{ws0}$ ), activation volumes, and activation compressibilities as described earlier.

The temperature dependence of the relaxation rates was calculated as the apparent rates during the 1000 to 20 bar re-equilibration step at temperatures of T = 278.1, 283.1, 288.1, and 291.1 K. The change of relative population ([SLIP]/[WT]) over time was fit to a single exponential with the apparent rate of

$$k_{app} = k_{ws} + k_{sw} \tag{9}$$

An Eyring relationship between rate and temperature was found by plotting  $ln(k_{app}/T)$  against 1/T. The plot was fit to a linear equation to extract the entropic and enthalpic contributions of activation energy of transition from SLIP to WT during relaxation at 20 bar.

For the pressure-dependent unfolding experiments, <sup>15</sup>N/<sup>1</sup>H HSQC spectra at different pressures were collected, maximum peak intensities in each spectrum were obtained and compared with the peaks corresponding to the same residues collected at different pressures.

Overlapping peaks were excluded from the analysis. The intensity averages at different pressures were plotted as a function of pressure, and fit to a two-state unfolding model with XMGrace (47, 48),

$$\frac{I}{I_0} = \frac{e^{-\left(\Delta G_f^0 + P\Delta V_f\right)/RT}}{1 + e^{-\left(\Delta G_f^0 + P\Delta V_f\right)/RT}}$$
(10)

where  $I_0$  is the peak intensity at initial (20 bar) pressure, R is gas constant, and T is temperature.

The apparent volume difference between the folded and unfolded state ( $\Delta V_f$ ) and the free energy of folding ( $\Delta G_f^0$ ) were extracted. For simplicity, the max and min plateau values were set to 1 and 0.

For the pressure-jump <sup>15</sup>N/<sup>1</sup>H HSQC experiments, we analyzed the peaks under different pressures and determined the change in chemical shifts and intensities under pressures compared to the reference chemical shifts (positions of peaks at 20 bar). We fit the change in chemical shifts to the following equation to determine the nonlinear coefficients(18, 26, 49):

$$\Delta \delta_i = b_i \Delta p + c_i \Delta p^2 \qquad (11)$$

Where p is pressure (bars),  $b_i$  (parts per million per bar) and  $c_i$  (parts per million per square bars) are the first and second order pressure dependence coefficients on chemical shifts for the ith residue. A large  $c_i$  value suggests high nonlinear response to pressure. Fittings were performed with the built-in pressure-analysis function of NMRViewJ (44). Residue-specific nonlinear coefficient differences between the two conformations were calculated by subtracting the absolute values of  $c_i$  corresponding to each conformation:

$$\Delta c_i = \left| c_{iwt} \right| - \left| c_{islip} \right| \tag{12}$$

Values were mapped to the crystal structure of WT ARNT PAS-B (32) and visualized withPyMOL (50).

#### **Void Volume Calculation**

Void volumes of ARNT PAS-B WT and SLIP conformations were calculated with the ProteinVolume software package by Chen and Makhatadze (51). Briefly, the total solvent-excluded volume of the protein is calculated by filling the space within the protein's molecular surface with 0.02 Å probes. The van der Waals volume is calculated with the same process but counting only the probes that are within the van der Waals radius of any atoms. The void volume V<sub>void</sub> is given by the difference between the two volumes calculated. Solution NMR structures of WT and SLIP were used for the calculation (29, 31), using the average void volume of all 20 conformers in these ensembles.

#### **RESULTS AND DISCUSSION**

#### **Equilibrium Analyses: Pressure Dependence of ARNT PAS-B Conformation Equilibrium**

We previously determined the solution and crystal structures of WT ARNT PAS-B and the solution structure of the F444Q/F446A/Y456T (TRIP) variant (29, 31, 32). By comparing the average void volumes of the two solution structure ensembles with ProteinVolume (51), we found that the SLIP conformation had approximately 600 Å<sup>3</sup> smaller void volume than WT, leading us to anticipate that the equilibrium between these conformations might be pressure sensitive. To test this possibility, we recorded <sup>15</sup>N/<sup>1</sup>H and <sup>13</sup>C/<sup>1</sup>H HSQC spectra of ARNT PAS-B Y456T at increasing pressures (20, 250, 500, ... up to 2500 bar). Overlaying these spectra (**Fig. 2A, S1**), we noticed that signals from all three (<sup>1</sup>H, <sup>15</sup>N, <sup>13</sup>C) nuclei showed pressure-dependent chemical shift and intensity differences between the two conformations, as predicted from the volume differences between them. In general, we observed that increased pressure decreased the intensities of WT signals while concomitantly increasing SLIP signal intensities with good reversibility (**Fig. S2**), confirming the smaller calculated volume of the SLIP conformation (30).

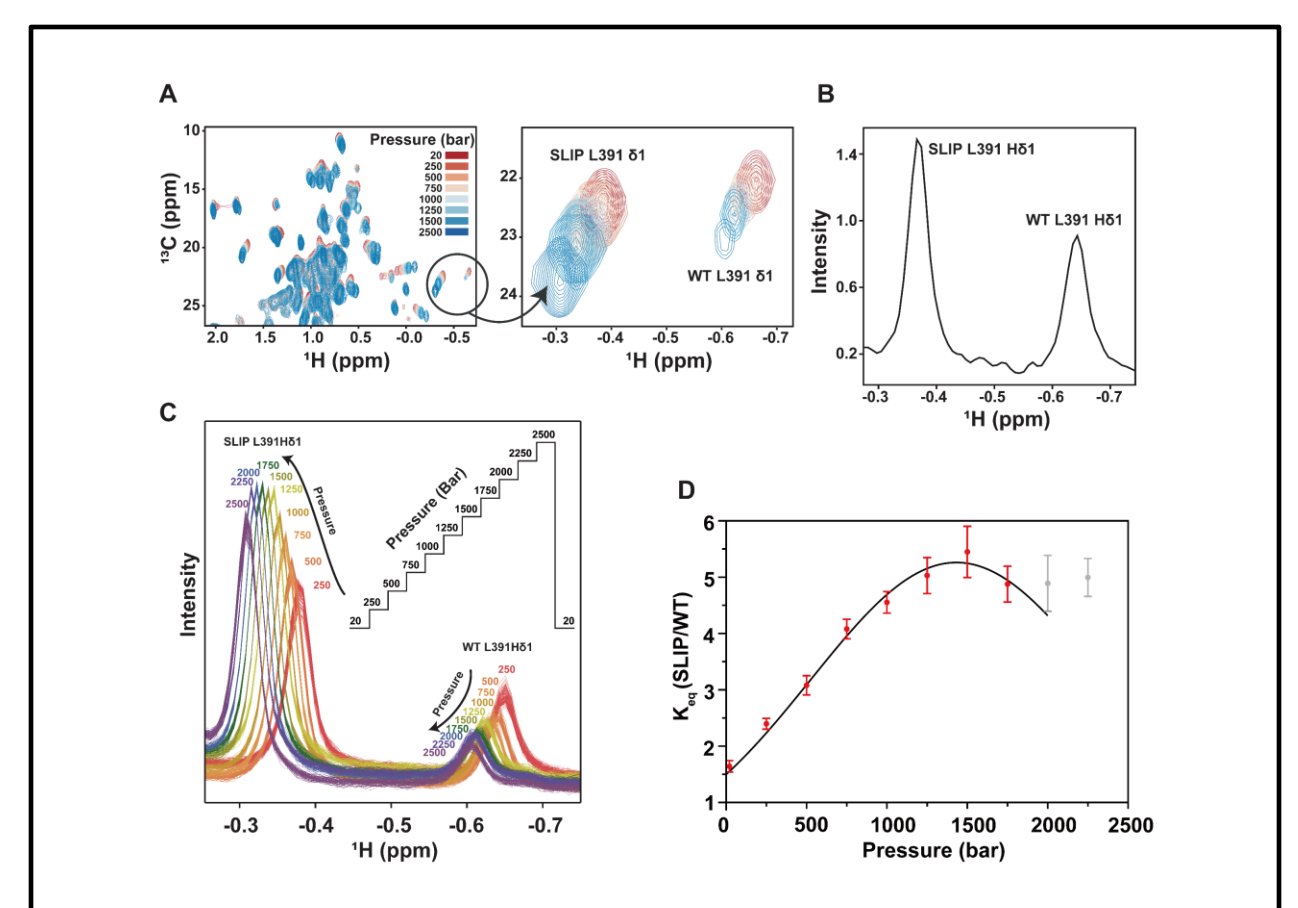


**Figure 2. NMR evidence for pressure-induced equilibrium shifts between WT and SLIP conformation of ARNT PAS-B Y456T.** A) Methyl region of  $^{13}$ C/ $^{1}$ H HSQC spectra of ARNT PAS-B Y456T recorded after equilibration between 20-2500 bar. Pressure-dependent intensity changes at several sites, including the L391 δ1 methyl group, reflect a shift in the SLIP:WT equilibrium. B)  $^{13}$ C-edited 1D  $^{1}$ H spectra of L391 Hδ1 equilibrated at 278.1K and 20 bar.  $K_{eq}$  (SLIP: WT) is approximately 1.5, as assessed by the areas of the two conformer-specific peaks. C)  $^{13}$ C-edited 1D  $^{1}$ H NMR of L391 Hδ1 recorded at pressures between 20-2500 bar as shown in inset. Spectra were collected during sample equilibration at each pressure. D) Fitting pressure dependence of equilibrated  $K_{eq}$  from datasets shown in C.  $K_{eq}$  above 1750 bar are not included for the fitting as another SLIP peak moves close to SLIP L391 δ1, interfering with the baseline and leading to overestimation of the SLIP population.

To characterize the thermodynamics and kinetics of the WT:SLIP conformational interconversion, we acquired a series of  $^{13}$ C-edited 1D  $^{1}$ H NMR spectra as the system equilibrated after pressure changes. We have previously shown that the upfield-shifted L391 Hδ1 methyl signal of both WT and SLIP conformations are well resolved in multiple types of NMR spectra, likely due to its location adjacent to a cavity only found in the WT conformation (**Fig. S3**) (30). Using this methyl group as a probe, we determined the equilibrium constant  $K_{eq}$  (=[SLIP]/[WT]) at different pressures (20 to 2500 bar) by measuring the ratios of the peak

integrals corresponding to these two conformations (**Fig. 2B, C**). Of note, we performed all experiments at 278.1K instead of room temperature to slow down the interconversion process, and thus improving the temporal resolution of the subsequent kinetic analysis.

275

276

277

278

279

280

281

282

283

284

285

286

287

288

289

290

291

292

293

294

295

296

297

From these data, we extracted the pressure dependence of  $K_{eq}$ , noting that it monotonically increased until approximately 1500 bar. Beyond 1500 bar, we observed that it remained approximately constant, showing that  $K_{eq}$  does not scale exponentially with pressure and correspondingly that the free energy  $\Delta G$  is not linearly dependent on pressure p (Eq. 1 and Fig. 2D), necessitating the inclusion of a nonlinear compressibility term for our analyses. Fitting these data to obtain differences in free energy between the two conformations at ambient pressure (referenced to 1 bar,  $\Delta G^0$ ), volume ( $\Delta V^0$ ), and compressibility ( $\Delta \beta V^0$ ) (Eq. 3), we found that the SLIP conformation was 40.5 ml/mol smaller than the WT conformation, agreeing reasonably with the ca. 105  $Å^3$  (= 63 ml/mol) internal cavities unique to the WT structure. We note that these values differ from the  $\sim 600 \text{ Å}^3$  void volume difference calculated above (=  $\sim 360$ ml/mol) from the WT and SLIP structures, as the experimentally-measured value includes contributions from both protein and solvent effects. Additional support for the pressure-driven loss of these cavities came from the measurement that the WT conformation was more compressible than the SLIP by 0.0285 ml/(mol bar). We attribute both the volume and compressibility differences to the collapse of internal cavities and increased packing accompanying the WT to SLIP transition (29, 32).

Finally, we compared the pressure-dependent *Keq* changes of several other cavity-oriented side chain methyl groups that can be readily identified with  $^{13}$ C/ $^{1}$ H HSQC experiments (L391  $\delta$ 2, L408  $\delta$ 1, M439  $\epsilon$ , shown in **Fig. S4**), and found that they all exhibit similar behavior as L391  $\delta$ 1, with negative volume (ranging from -20 to -36 ml/mol) and compressibility (ranging

from -0.012 to -0.025 ml/(mol bar)) changes upon WT to SLIP transition. We note that identifying peak pairs that are not interfered by other peaks at multiple pressure points is challenging, and further studies are warranted to investigate the intrinsic variability of the thermodynamic parameters among different residues.

## Pressure Jump Kinetic Analyses: WT and SLIP Interconvert by Transitioning into an Intermediate State with Small Volume and Compressibility

To complement the above equilibrium pressure analyses, we used a pressure jump protocol to obtain complementary kinetics measurements. To do so, we jumped the sample pressure from 20 bar to various higher values, acquiring 1D <sup>13</sup>C-edited <sup>1</sup>H NMR spectra as the system re-equilibrated and measuring the populations of the two conformations by the area of the respective L391 Hδ1 signals (**Fig. 3A**). Notably, we conducted these studies with commercially-available instrumentation capable of completing even the largest of these jumps within 30-60 sec, making it possible for us to perform the kinetic analyses due to the slow kinetics of the interconversion process (**Fig. 3A**). Custom-built, NMR-compatible pressure systems have recently been reported which are capable of such jumps approximately 100-fold faster (23, 24).

As an initial control of this approach, we extracted the  $K_{eq}$  values from these direct jump experiments and fit them for the same parameters mentioned in the equilibrium analyses (**Fig. S5**). This yielded a  $\Delta V^0$  of -46.1 ml/mol, and a  $\Delta \beta V^0$  of -0.0433 ml/(mol bar) (**Table 1**), comparable to values we noted above. While direct pressure jumps may induce convergence of  $K_{eq}$  at a slightly lower pressure, as indicated by the bigger difference in compressibilities between the two states, we otherwise believe that these values are similar despite different experimental routes.

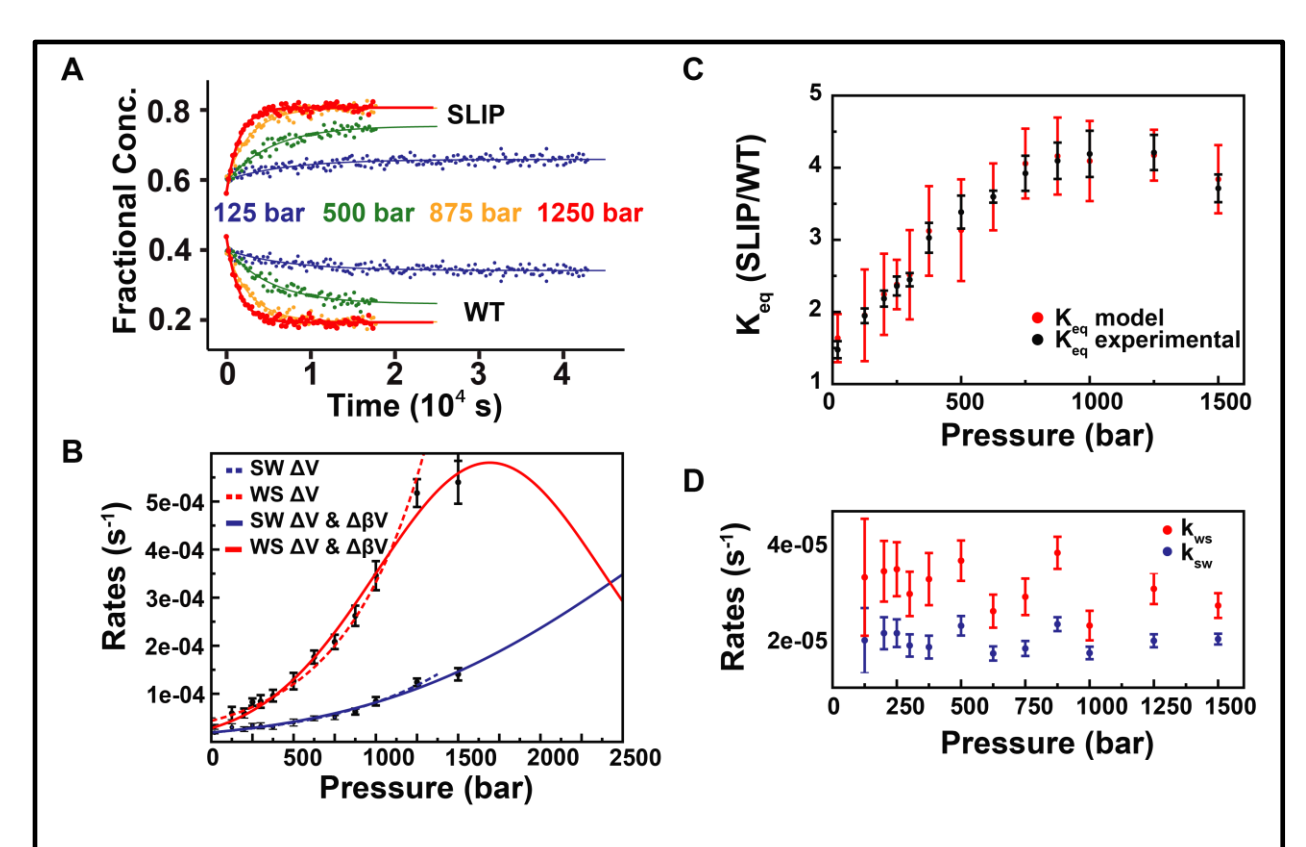


**Figure 3. Kinetic analysis of the ARNT PAS-B interconversion.** A) Examples of independent fits of the rate constants using the L391 H81  $^{1}$ H methyl signals at the indicated pressures. Total population of the WT and SLIP was normalized to 1 for each analysis. B) Fitting of the decoupled rates ( $k_{sw}$  in blue,  $k_{ws}$  in red) as functions of pressure. Two models (without and with compressibility implemented) were used to fit the experimental data, using dashed (solid) lines to indicate fits without (with) compressibility included. C) Comparison of fit model (red) to experimental data (black). Equilibrium constants from the model are calculated from the rates derived from the kinetic analysis. D) Decoupled rates of relaxation. Each rate pair is plotted against the pressure the system was relaxed from. Relaxation rates appear to be independent of the initial pressure.

To analyze the kinetics of the interconversion process, we assumed that a two-state model could be applied by our prior observation that the intermediate state of ARNT PAS-B Y456T is only transiently visited during interconversion (30). We validated this assumption by establishing that the sum population of the two states remained constant at pressures below 2500 bar, suggesting the intermediate is not accumulating (**Fig. S6**). In the two-state transition model, the apparent exchange rate is the sum of the two rate constants corresponding to the individual transitions from SLIP to WT and vice-versa ( $k_{app} = k_{ws} + k_{sw}$ , **Eq. 9**) (52). To obtain the pressure dependence on both rates, we initially fit the apparent exchange rate vs. pressure to a

biexponential equation (**Eq. 4**), to yield the initial rates at 1 bar ( $k_{sw0}$  and  $k_{ws0}$ ), the activation volumes ( $\Delta V_{sw}^{\ddagger}$  and  $\Delta V_{ws}^{\ddagger}$ ), and the activation compressibilities ( $\Delta \beta V_{sw}^{\ddagger}$  and  $\Delta \beta V_{ws}^{\ddagger}$ ). To avoid needing to simultaneously fit six parameters, we decoupled the two rates by solving them numerically under different pressures as described in Materials and Methods (**Eq. 5**, **6**; **Fig. S7**, **S8**). This allowed us to independently fit each rate as a function of pressure with three parameters (**Eq. 7**, **8**; **Fig. 3A**, **B**), summarized in **Table 1**.

Table 1. Summary of the kinetic and thermodynamic parameters derived from pressure-induced interconversion and unfolding of ARNT PAS-B variants

Thermodynamic Analyses		Kinetic Analyses	
SLIP – WT, step jumps <sup>a</sup>		with ΔβV	
ΔV <sup>0</sup> (ml/mol)	$-40.5 \pm 0.47$	ΔV <sup>‡</sup> <sub>SW</sub> (ml/mol)	$-37.6 \pm 3.0$
ΔβV° (ml/(mol bar))	$-0.0285 \pm 0.00065$	ΔV <sup>‡</sup> <sub>WS</sub> (ml/mol)	-82.4 ± 7.4
SLIP – WT, direct jumps <sup>b</sup>		$\Delta \beta V_{SW}^{\ddagger}$ (ml/(mol bar))	$-0.00875 \pm 0.0034$
ΔV <sup>0</sup> (ml/mol)	-46.1 ± 0.41	$\Delta \beta V_{WS}^{\ddagger}$ (ml/(mol bar))	$-0.0487 \pm 0.0066$
ΔβV° (ml/(mol bar))	$-0.0433 \pm 0.00067$	without ΔβV	
Unfolding (U - F)		ΔV <sup>‡</sup> <sub>SW</sub> (ml/mol)	$-32.8 \pm 0.62$
WT (ml/mol)	$-126.3 \pm 3.1$	ΔV <sup>‡</sup> <sub>WS</sub> (ml/mol)	-59.0 ± 1.38
TRIP (ml/mol)	-83.3 ± 2.3		

Uncertainties were estimated by bootstrapping. Random noises with mean of 0 and variance of the standard error were added to the raw data and fit repeatedly for  $n\ge30$  times to determine the 95% confidence interval. <sup>a</sup> step jumps – jumping pressure incrementally with 250 bar steps. <sup>b</sup> direct jumps – jumping pressure directly from 20 bar to various high pressures.

From these analyses, we observed negative activation volumes and compressibilities for both transitions, implying that they proceed through an intermediate state which is both smaller and less compressible than the starting conformations. Moreover, the magnitude of the volume barrier is bigger for the WT to SLIP transition, with a 44.8 ml/mol difference in activation volumes, consistent with the 40.5 ml/mol volume difference obtained from the thermodynamic

analysis. Taking the ratios of the two rate constants ( $k_{ws}/k_{sw}$ ) at different pressures yielded equilibrium constants matching experimental data (**Fig. 3C**). Since both activation volumes were negative, the transition rates were correspondingly accelerated under pressure. Interestingly, the activation volume for the WT to SLIP transition (-82.4 ml/mol, or 137 Å<sup>3</sup>/molecule) is strikingly similar to the cavity size of the WT conformation. The SLIP to WT transition, in contrast, required a much smaller activation volume (**Table 1**). While the pressure-induced volume change of a system is a combined effect from compressing both protein and solvent (20), we found a positive correlation between cavity size and activation volume. From these data, we postulate the transition between the two confirmations requires the protein to collapse its internal cavities and voids to reduce its total volume, consistent with substantial unfolding that we quantitate below. This claim is further supported by Roche *et al.*'s (53) recent work highlighting that pressure-driven protein unfolding is a result of cavity elimination.

Additional support for an unfolded transition state is provided by the negative activation compressibilities, as the replacement of interatomic contacts with hydration shells during unfolding will substantially reduce compressibility (54). Notably, as compressibility is small and neglectable at lower pressures (18), we were able to fit the sub-1000 bar data points to a model without compressibility, leading to the same observation that the SLIP conformation is smaller than the WT conformation, albeit to a lesser extent (**Fig. 3B**; **Table 1**).

### Pressure Induced Interconversion is Reversible and Provides Thermodynamic Information on Transition State

To validate the reversibility of the pressure-jump experiments, we recorded  $^{13}$ C-edited 1D  $^{1}$ H NMR spectra as samples were dropped from higher pressures down to 20 bar. From these data, we extracted the two rate constants  $k_{ws}$  and  $k_{sw}$  and plotted them against the pressures prior

to 1500 bar), the relaxation rates remained the same and the corresponding [SLIP]/[WT] equilibrium constants were the same as we measured in equilibrium studies at 20 bar. These results, together with our comparison of <sup>15</sup>N/<sup>1</sup>H HSQC spectra recorded before and after pressure-jump experiments (**Fig. S2**), provide important experimental controls by establishing that this system is both thermodynamically and kinetically reversible up to at least 1500 bar and that interconversion rates are solely determined by the applied pressure (and not susceptible to hysteresis effects of prior pressure applications).

As an additional verification of the suitability of pressure jumps for kinetic studies of this process, we compared the parameters extracted from these pressure-jumped measurements to those from an Eyring analysis of the rates of interconversion determined after chromatographic isolation of one of the two conformers (30). To do so, we equilibrated the protein at 1000 bar at four different temperatures between 278.1 and 291.1K, then relaxed the system to 20 bar and recorded <sup>13</sup>C-edited 1D <sup>1</sup>H NMR spectra to extract the apparent exchange rates from SLIP to WT (**Fig. S9**). From Eyring analysis of these data, we extracted entropic (-47.8 cal/(mol degree) = -14.2 kcal/mol at 298K) and enthalpic (7.4 kcal/mol) contributions to the activation energy, which are similar to our previously-reported results with chromatographic perturbations (30). These data both support interconversion via an unfolded transition state, as indicated by the large entropic barrier, and more generally demonstrate that the relaxation process we monitored here after pressure perturbation is the same as we previously observed with chromatographic separation (29, 30).

### Activation Volumes of the ARNT PAS-B Y456T are Comparable to the Unfolding Volumes of the WT and TRIP Variant Detected by Pressure Jump NMR

383

384

385

386

387

388

389

390

391

392

393

394

395

396

397

398

399

400

401

402

403

404

To calibrate the degree of unfolding involved in the ARNT PAS-B Y456T transition state, we compared the activation volumes of interconversion to the unfolding volumes of the WT and SLIP conformations (as adopted by the WT and TRIP variant). As neither protein substantially unfolded within our 2500 bar experimentally-accessible pressure range, we added 3 M urea to slightly lower the stability of both samples. From <sup>15</sup>N/<sup>1</sup>H HSQC spectra we acquired at different pressures in the presence of this denaturant, it was clear that all the resolved backbone peaks showed pressure-induced reductions in intensity, with no obvious peak broadening (Fig. **S10**). This was accompanied by the appearance of intense peaks with sharp linewidths and poor <sup>1</sup>H chemical shift dispersion, consistent with pressure-induced protein unfolding that completed at approximately 1750 bar (WT) and 2500 bar (TRIP) (Fig. 4A, S10). By fitting the protein unfolding curves for both proteins to a two-state model (Eq. 10, Fig. 4B), we extracted two key parameters: the average volume difference between the folded and the unfolded protein  $(\Delta V_f)$ and the free energy of folding  $(\Delta G_f^0)$  (20, 55) (**Table 1**). The unfolding volumes indicate a 43.0 ml/mol difference between the two folded structures, and the folding energies predict a 2.7:1 ratio between the SLIP and the WT conformation at ambient pressure, both similar to what we observed for ARNT PAS-B Y456T (40.5 ml/mol and 1.5:1, respectively). The activation volumes of the ARNT PAS-B Y456T, which represent the volume differences between the two folded states to the intermediate state, are smaller but comparable to the unfolding volumes of the WT and TRIP variant (-82.4 ml/mol vs. -126.3 ml/mol for WT, -37.6 ml/mol vs. -83.3 ml/mol for SLIP). These data, coupled with the correlation between the interconversion and

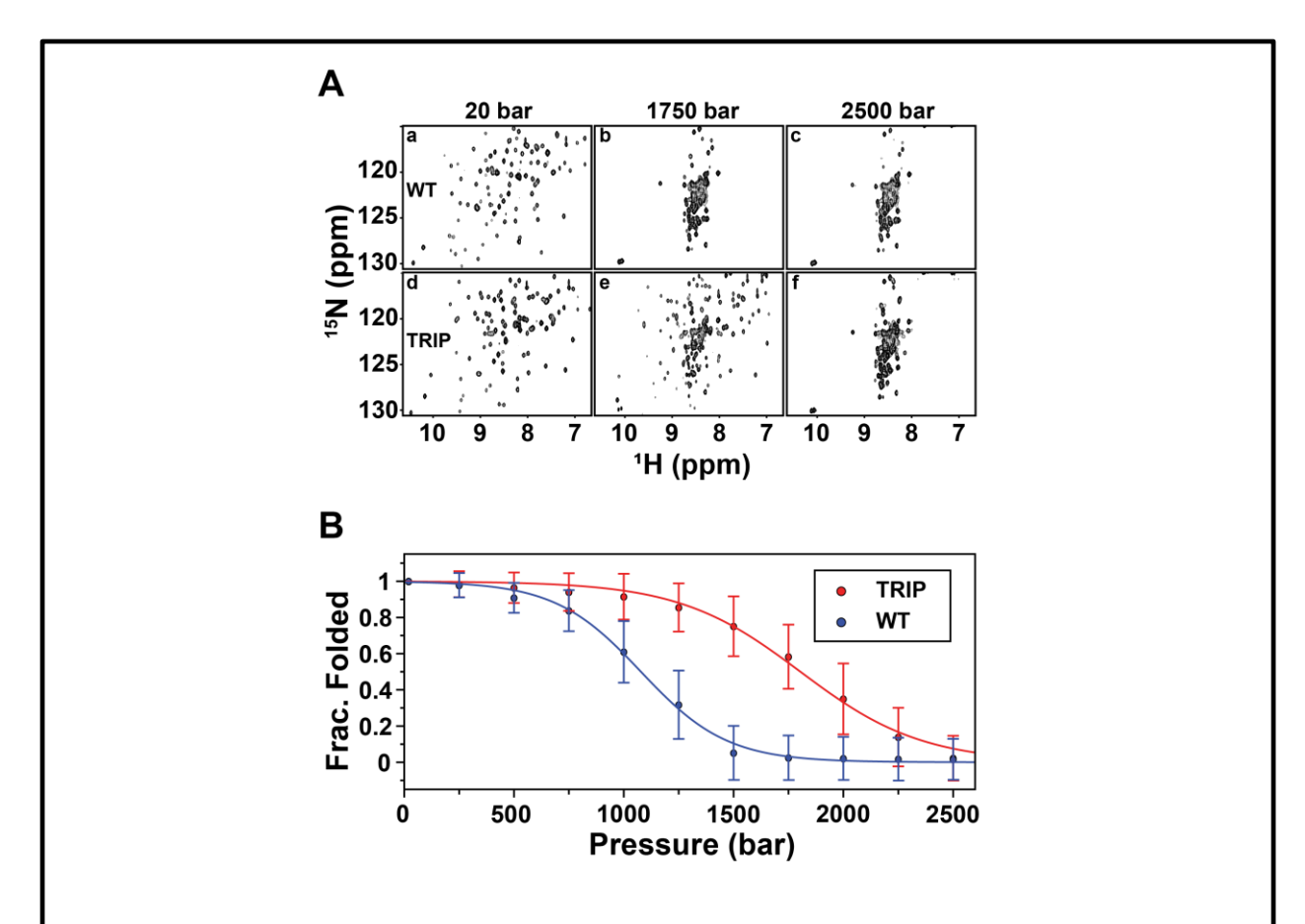


**Figure 4.** Unfolding profile of ARNT PAS-B WT and TRIP mutant detected by high-pressure NMR <sup>15</sup>N/<sup>1</sup>H HSQC at 278 K and 3.0 M urea. A) Example <sup>15</sup>N/<sup>1</sup>H-HSQC spectra of WT and TRIP at different pressures. (a-c) NMR spectra of WT at initial pressure (20 bar), intermediate pressure (1750 bar), and final pressure (2500 bar). (d-f) NMR spectra of TRIP mutant. B) Average unfolding curves for ARNT PAS-B WT and TRIP mutant. Peak intensities are normalized between 0 and 1.

denaturant-free protein unfolding rates we previously reported (30) and the need to significantly remodel at least 15 of 26 inter-strand hydrogen bonds in the beta sheet, lead us to strongly support a model where ARNT PAS-B Y456T largely unfolds as it interconverts between conformations.

We additionally compared the unfolding volumes of WT and TRIP to the unfolding volumes of similarly-sized proteins (10-20 kDa). Indeed, the numbers are in good agreement with several other proteins studied with pressure-dependent unfolding approaches, as

summarized in **Table S1** (42, 53, 56-60). A schematic figure describing the relationships among the two folded conformations, the intermediate state, and the unfolded state is shown in **Fig. 5**.

**Cavity Locations** 

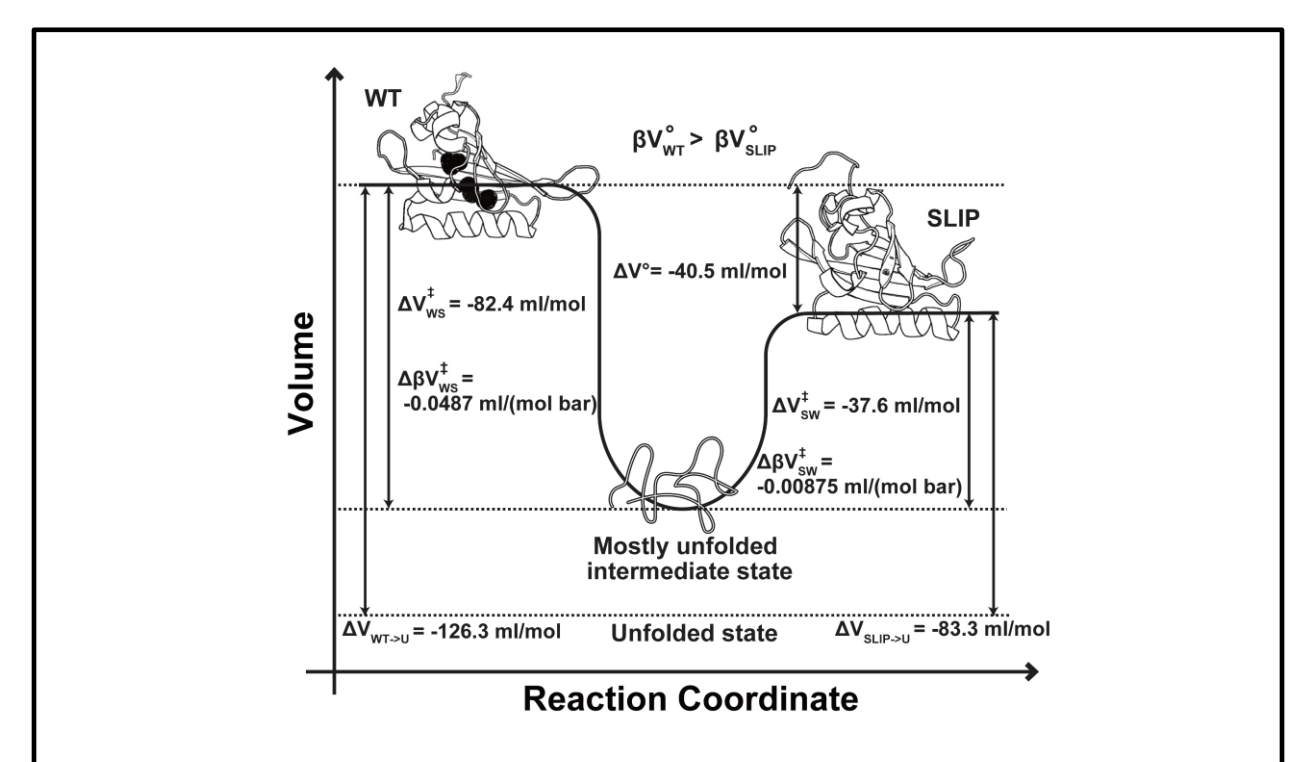


**Figure 5. Summary of the volume and compressibility parameters of the folded and unfolded states of ARNT PAS-B Y456T.** Schematic representation comparing the folded, intermediate, and unfolded states of ARNT PAS-B Y456T. The listed parameters and additional information are provided in **Table 1**.

Lastly, we note that we did not include compressibility changes for the unfolding analysis of ARNT PAS-B WT and TRIP, given that these were based on global averages of signals (> 60 residues) distributed throughout both proteins which we assume to average out contributions from sites near cavities (compressibility-dependent) and those far from cavities (compressibility-independent) (18, 28).

### Pressure-induced Nonlinear Chemical Shift Changes and Residue Compressibilities Predict

Certain types of pressure-induced NMR chemical shift changes have been related to conformational changes within proteins (26, 27). In particular, non-linear shift changes are

hallmarks of such conformational changes, as identified by fitting chemical shifts to pressure using a linear and a nonlinear term (**Eq. 11**) (18). Of particular interest is the nonlinear coefficient ( $c_i$ ) of the backbone amide <sup>15</sup>N and <sup>1</sup>H nuclei, where larger values are particularly sensitive on the ability of proteins to visit multiple conformational states upon application of pressure. Such information can be analyzed in bulk, with larger average  $c_i$  values or broader  $c_i$  distributions reflecting the presence of internal cavities or voids which enable protein flexibility with increased pressure (18, 26, 28, 49). At a residue-specific level, larger  $c_i$  values tend to be observed from residues located near internal cavities (18, 28).

423

424

425

426

427

428

429

430

431

432

433

434

435

436

437

438

439

440

441

442

443

444

445

To test if this trend holds for the WT and SLIP conformations of ARNT PAS-B, we acquired <sup>15</sup>N/<sup>1</sup>H HSQC spectra of both WT and TRIP samples of ARNT PAS-B at pressures up to 2000 bar (Fig. 6A). We fit the pressure-dependent changes in <sup>15</sup>N chemical shifts of assignable residues to Eq. 11, using these to extract  $^{15}$ N  $c_i$  values for both conformations (Fig. **6B**) (29, 31). While the two conformers have similar overall structures, we observed markedly different distributions of the backbone amide  $^{15}$ N  $c_i$  values. Specifically, we observed a global reduction of the magnitude of  $c_i$  in the SLIP conformation, supporting the view that it has reduced internal void volume and flexibility compared to the WT conformation. We calculated the differences in nonlinear coefficients by subtracting the absolute values of  $c_i$  of the SLIP conformation from the WT conformation (Eq. 12). Residues with the largest  $^{15}$ N  $c_i$  differences were located near the internal cavities or on loops of the WT structure (Fig. 6C), with many clustered into two regions of the protein (Fig. 6B). Intriguingly, the same clusters of residues have also been associated with the binding of KG-548 to ARNT PAS-B, disrupting interactions between ARNT PAS-B and the TACC3 co-activator (32). The cavities apparently collapse in the SLIP conformation due to the +3 shift and inversion of the Iβ-strand, resulting in a more packed

local environment, explaining the substantial  $c_i$  reduction of these residues in the SLIP conformation. Interestingly, residue Y456, the site of the Y456T point mutation that creates the SLIP conformation, has one of the largest <sup>15</sup>N  $c_i$  difference between the two conformations.

446

447

448

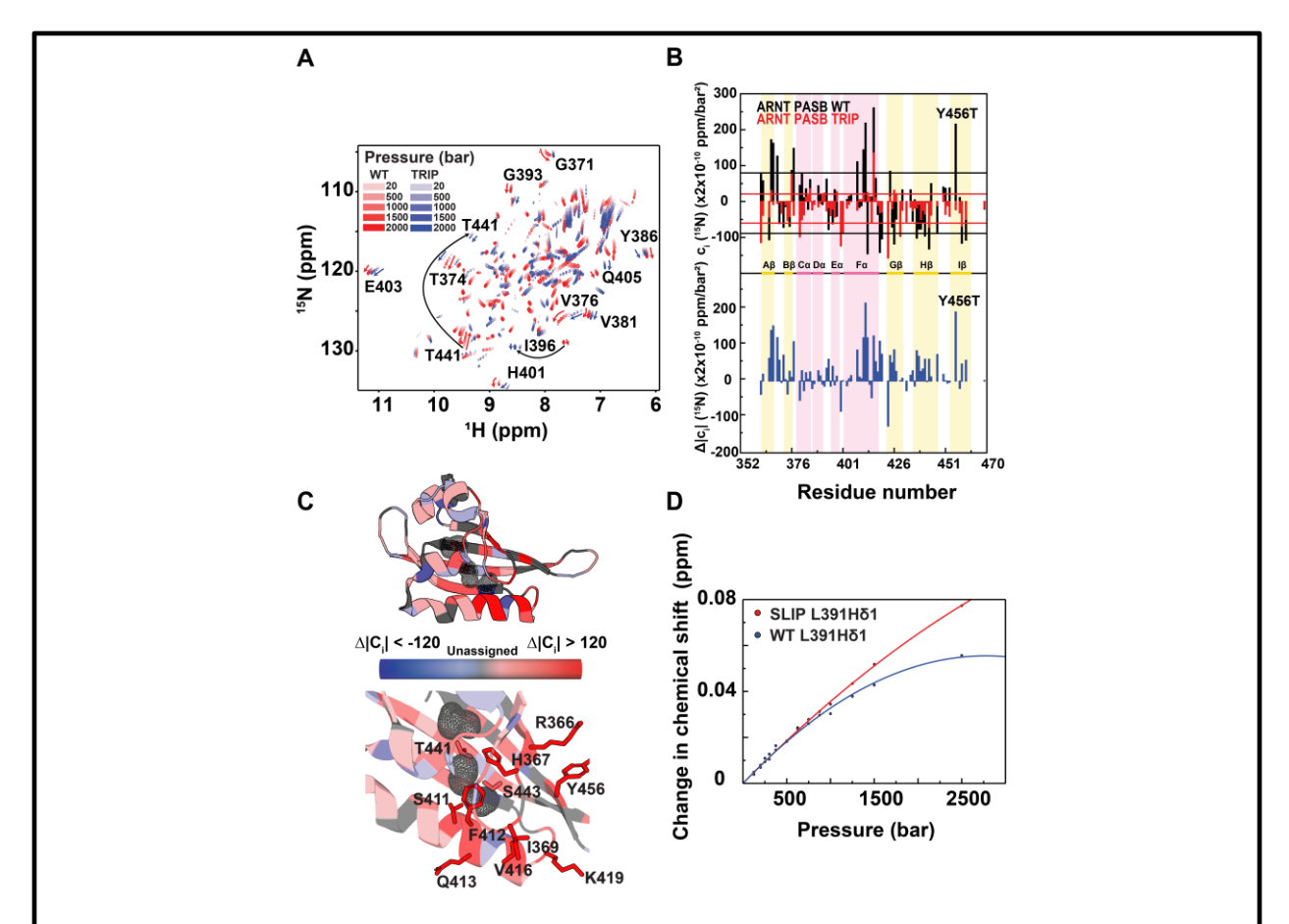


Figure 6. Residues surrounding cavities of ARNT PAS-B are rigidified in the SLIP conformation. A) <sup>15</sup>N/<sup>1</sup>H HSQC spectra of WT and TRIP variant ARNT PAS-B under pressures from 20 to 2000 bar, showing large chemical shift differences between conformations despite high structural similarities between the two. Pressure-dependent non-linear chemical shift changes are also different between WT and SLIP, which are highlighted by red and blue arrows for several example residues. B) Pressure-dependent non-linear chemical shift changes of the two conformations as measured by  $^{15}$ N  $c_i$  (top panel) and differences in non-linearities between the two conformations ( $|WT c_i|$ - $|SLIP c_i|$ ) (bottom panel) mapped onto the sequence and secondary structure of WT ARNT PAS-B. The standard deviation of WT  $c_i$  (black lines,  $84 \times 2 \times 10^{-10}$  ppm/bar<sup>2</sup>) is about 2 times the standard deviation of SLIP  $c_i$  (red lines,  $41 \times 2 \times 10^{-10}$  ppm/bar<sup>2</sup>). C) Mapping the residue-specific differences in non-linear coefficients between WT and SLIP suggest that WT is globally more dynamic. Residues with large non-linear coefficient differences ( $\Delta c_i > 120$ ) between WT and SLIP (366, 367, 369, 411, 412, 413, 416, 419, and 456) are located near the cavities (gray mesh) or on loop regions of WT ARNT PAS-B. Other residues oriented toward cavities (i.e. T441 and S443) also show more non-linear chemical shift changes in WT than SLIP. D) <sup>1</sup>H chemical shift changes of L391 H81 for both the WT and SLIP conformations of ARNT PAS-B Y456T are plotted against pressure. The chemical shift change of the residue in the WT conformation shows remarkably more non-linear characteristic than it is in the SLIP conformation.

We suspected that the residue-specific compressibility also depends on whether the residue is near a cavity. As expected, when we fit the pressure dependence of the L391 H81 peak to **Eq. 11**, we obtained a larger nonlinear coefficient for the WT conformation than the SLIP conformation (**Fig. 6D**), matching the compressibility difference observed between the two states, confirming our speculation. We also compared the pressure-dependent responses of several other methyl peaks corresponding to the WT and SLIP conformations using the  $^{13}$ C/ $^{1}$ H-HSQC spectra of ARNT PAS-B Y456T (**Fig. S11**). We found several cavity-oriented methyl groups to have markedly larger  $^{1}$ H or  $^{13}$ C  $c_i$  values for the WT conformation (L391  $\delta$ 2, I396  $\delta$ 1, L408  $\delta$ 1 and  $\delta$ 2, and M439  $\varepsilon$ ). Correspondingly, the pressure-dependent WT to SLIP transitions were also slowed down at higher pressures as the result of negative compressibility changes, similar to L391  $\delta$ 1 (**Fig. S4**).

Since both nonlinear chemical shift changes and compressibility probe for the volume-dependent local environment a residue resides in, measuring the nonlinear coefficient of chemical shift changes and compressibility can complement each other for more accurate characterization of cavities in proteins (as has been linked mathematically in the past (61)). This is in line with the prior notion that larger compressibility is correlated with larger volume fluctuations, which are generally observed near cavities, where residues are less tightly packed (62). Remarkably, the cavities in the WT ARNT PAS-B were not initially observed in the solution structure (31), showing the potential of pressure-NMR as the means of rapidly identifying smaller cavities from moderate resolution structures where cavities and/or ligand binding pockets are not obvious (31).

#### CONCLUSION

470

471

472

473

474

475

476

477

478

479

480

481

482

483

484

485

486

487

488

489

490

491

The shift of the β-strand register at an interaction interface enabled by a single point mutation is mechanistically intriguing and raises fundamental questions about the relative stabilities of the ground state and energetically close alternate conformers (30, 63, 64). Using 1D and 2D pressure-jump NMR experiments, we examined one such case by elucidating the volume and compressibility differences between two stably folded conformations of ARNT PAS-B which interconvert when enabled by a single point mutation, Y456T. We demonstrated that the wildtype (WT) state has a substantially larger internal volume and compressibility compared to the alternate slip conformation (SLIP), and that these differences can be largely attributed to the cavities unique to the WT state. Furthermore, we show that interconversion between the two states goes through a chiefly-unfolded intermediate state that is smaller in volume and compressibility than both folded conformations. Additionally, we found a possible connection between residue-specific compressibility and NMR nonlinear chemical shift responses to pressure that could help to predict whether residues are located close to cavities. While promising, we emphasize that a more comprehensive analysis is required to validate this hypothesis.

In summary, we have shown how varying pressure can be easily applied to reversibly shift the equilibrium of a protein between two stably folded conformations, letting us quantitatively measure structural and thermodynamic parameters otherwise difficult to access (20). We believe that this approach can be applied to other proteins which undergo large scale conformational changes, particularly with recent instrumentation advances that allow millisecond-timescale pressure jumps (23, 24). We anticipate that such studies will be

particularly useful studying systems where protein flexibility is essential, including enzymatic conformational changes, protein/ligand interactions, and metamorphic systems (9-11).

#### **SUPPORTING MATERIAL**

494

496

499

500

501

502

503

504

Supplementary Table S1; Figures S1-S11.

#### **AUTHOR CONTRIBUTIONS**

497 X.X, D.G, J.M.A, and K.H.G designed the experiments; X.X, J.M.A, and D.G performed 498 the experiments; X.X and K.H.G. analyzed the data and wrote the manuscript.

#### **ACKNOWLEDGEMENTS**

This work was supported by NSF grant MCB 1818148 (K.H.G.) and Fonds de Recherche Québec – Nature et Technologie fellowship B3X (D.G.). We thank Bruce Johnson (CUNY ASRC) for developing new extensions of the NvFX software package (44, 45) for pressure NMR analysis, and members of the Gardner laboratory for constructive comments.

#### REFERENCES

- Leopold, P. E., M. Montal, and J. N. Onuchic. 1992. Protein folding funnels: a kinetic approach to the sequence-structure relationship. Proc Natl Acad Sci U S A 89(18):8721-8725.
- Onuchic, J. N., H. Nymeyer, A. E. Garcia, J. Chahine, and N. D. Socci. 2000. The energy landscape theory of protein folding: insights into folding mechanisms and scenarios. Adv Protein Chem 53:87-152.
- Ishikawa, H., K. Kwak, J. K. Chung, S. Kim, and M. D. Fayer. 2008. Direct observation of fast protein conformational switching. Proc Natl Acad Sci U S A 105(25):8619-8624.

- 513 4. Tuinstra, R. L., F. C. Peterson, S. Kutlesa, E. S. Elgin, M. A. Kron, and B. F. Volkman.
- 514 2008. Interconversion between two unrelated protein folds in the lymphotactin native
- state. Proc Natl Acad Sci U S A 105(13):5057-5062.
- 516 5. Ha, J. H., and S. N. Loh. 2012. Protein conformational switches: from nature to design.
- 517 Chemistry 18(26):7984-7999.
- 518 6. Zoltowski, B. D., C. Schwerdtfeger, J. Widom, J. J. Loros, A. M. Bilwes, J. C. Dunlap,
- and B. R. Crane. 2007. Conformational switching in the fungal light sensor Vivid.
- Science 316(5827):1054-1057.
- Harper, S. M., L. C. Neil, and K. H. Gardner. 2003. Structural basis of a phototropin light
- switch. Science 301(5639):1541-1544.
- 523 8. London, R. E. 2019. HIV-1 Reverse Transcriptase: A Metamorphic Protein with Three
- 524 Stable States. Structure 27(3):420-426.
- 9. Murzin, A. G. 2008. Biochemistry. Metamorphic proteins. Science 320(5884):1725-
- 526 1726.
- 527 10. Yadid, I., N. Kirshenbaum, M. Sharon, O. Dym, and D. S. Tawfik. 2010. Metamorphic
- 528 proteins mediate evolutionary transitions of structure. Proc Natl Acad Sci U S A
- 529 107(16):7287-7292.
- 530 11. Agarwal, P. K., N. Doucet, C. Chennubhotla, A. Ramanathan, and C. Narayanan. 2016.
- Conformational Sub-states and Populations in Enzyme Catalysis. Methods Enzymol
- 532 578:273-297.
- 533 12. Brereton, A. E., and P. A. Karplus. 2015. Native proteins trap high-energy transit
- conformations. Sci Adv 1(9):e1501188.

- Loria, J. P., R. B. Berlow, and E. D. Watt. 2008. Characterization of enzyme motions by
- solution NMR relaxation dispersion. Acc Chem Res 41(2):214-221.
- 537 14. Alderson, T. R., and L. E. Kay. 2020. Unveiling invisible protein states with NMR
- spectroscopy. Curr Opin Struct Biol 60:39-49.
- 539 15. Scheuermann, T. H., D. R. Tomchick, M. Machius, Y. Guo, R. K. Bruick, and K. H.
- Gardner. 2009. Artificial ligand binding within the HIF2alpha PAS-B domain of the
- 541 HIF2 transcription factor. Proc Natl Acad Sci U S A 106(2):450-455.
- 542 16. Di Russo, N. V., D. A. Estrin, M. A. Marti, and A. E. Roitberg. 2012. pH-Dependent
- conformational changes in proteins and their effect on experimental pK(a)s: the case of
- Nitrophorin 4. PLoS Comput Biol 8(11):e1002761.
- 545 17. Caldwell, C. R. 1987. Temperature-Induced Protein Conformational Changes in Barley
- Root Plasma Membrane-Enriched Microsomes: II. Intrinsic Protein Fluorescence. Plant
- 547 Physiol 84(3):924-929.
- 548 18. Akasaka, K. 2006. Probing conformational fluctuation of proteins by pressure
- perturbation. Chem Rev 106(5):1814-1835.
- 550 19. Caro, J. A., and A. J. Wand. 2018. Practical aspects of high-pressure NMR spectroscopy
- and its applications in protein biophysics and structural biology. Methods 148:67-80.
- 552 20. Roche, J., and C. A. Royer. 2018. Lessons from pressure denaturation of proteins. J R
- 553 Soc Interface 15(147).
- 554 21. Akasaka, K., R. Kitahara, and Y. O. Kamatari. 2013. Exploring the folding energy
- landscape with pressure. Arch Biochem Biophys 531(1-2):110-115.

- 556 22. Liu, Y., M. B. Prigozhin, K. Schulten, and M. Gruebele. 2014. Observation of complete
- pressure-jump protein refolding in molecular dynamics simulation and experiment. J Am
- 558 Chem Soc 136(11):4265-4272.
- 559 23. Charlier, C., T. R. Alderson, J. M. Courtney, J. Ying, P. Anfinrud, and A. Bax. 2018.
- Study of protein folding under native conditions by rapidly switching the hydrostatic
- pressure inside an NMR sample cell. Proc Natl Acad Sci U S A 115(18):E4169-E4178.
- 562 24. Charlier, C., J. M. Courtney, T. R. Alderson, P. Anfinrud, and A. Bax. 2018. Monitoring
- 563 (15)N Chemical Shifts During Protein Folding by Pressure-Jump NMR. J Am Chem Soc
- 564 140(26):8096-8099.
- 565 25. Fuglestad, B., M. A. Stetz, Z. Belnavis, and A. J. Wand. 2017. Solution NMR
- investigation of the response of the lactose repressor core domain dimer to hydrostatic
- pressure. Biophys Chem 231:39-44.
- Akasaka, K., and H. Li. 2001. Low-lying excited states of proteins revealed from
- nonlinear pressure shifts in 1H and 15N NMR. Biochemistry 40(30):8665-8671.
- 570 27. Williamson, M. P., and R. Kitahara. 2019. Characterization of low-lying excited states of
- proteins by high-pressure NMR. Biochim Biophys Acta Proteins Proteom 1867(3):350-
- 572 358.
- 573 28. Gagné, D. A., R.; Edupuganti, U.R.; Williams, J.; Aramini, J.M.; Akasaka, K., Gardner,
- K.H. . 2020. Use of high pressure NMR spectroscopy to rapidly identify internal ligand-
- 575 binding voids in proteins. Manuscript under review.
- 576 29. Evans, M. R., P. B. Card, and K. H. Gardner. 2009. ARNT PAS-B has a fragile native
- state structure with an alternative beta-sheet register nearby in sequence space. Proc Natl
- 578 Acad Sci U S A 106(8):2617-2622.

- 579 30. Evans, M. R., and K. H. Gardner. 2009. Slow transition between two beta-strand registers
- is dictated by protein unfolding. J Am Chem Soc 131(32):11306-11307.
- 581 31. Card, P. B., P. J. Erbel, and K. H. Gardner. 2005. Structural basis of ARNT PAS-B
- dimerization: use of a common beta-sheet interface for hetero- and homodimerization. J
- 583 Mol Biol 353(3):664-677.
- 584 32. Guo, Y., C. L. Partch, J. Key, P. B. Card, V. Pashkov, A. Patel, R. K. Bruick, H. Wurdak,
- and K. H. Gardner. 2013. Regulating the ARNT/TACC3 axis: multiple approaches to
- manipulating protein/protein interactions with small molecules. ACS Chem Biol
- 587 8(3):626-635.
- 588 33. Guo, Y., T. H. Scheuermann, C. L. Partch, D. R. Tomchick, and K. H. Gardner. 2015.
- Coiled-coil coactivators play a structural role mediating interactions in hypoxia-inducible
- factor heterodimerization. J Biol Chem 290(12):7707-7721.
- 591 34. Wu, D., N. Potluri, J. Lu, Y. Kim, and F. Rastinejad. 2015. Structural integration in
- 592 hypoxia-inducible factors. Nature 524(7565):303-308.
- 593 35. Wu, D., X. Su, N. Potluri, Y. Kim, and F. Rastinejad. 2016. NPAS1-ARNT and NPAS3-
- 594 ARNT crystal structures implicate the bHLH-PAS family as multi-ligand binding
- 595 transcription factors. Elife 5.
- 596 36. Henry, J. T., and S. Crosson. 2011. Ligand-binding PAS domains in a genomic, cellular,
- and structural context. Annu Rev Microbiol 65:261-286.
- 598 37. Partch, C. L., P. B. Card, C. A. Amezcua, and K. H. Gardner. 2009. Molecular basis of
- coiled coil coactivator recruitment by the aryl hydrocarbon receptor nuclear translocator
- 600 (ARNT). J Biol Chem 284(22):15184-15192.

- And A. Partch, C. L., and K. H. Gardner. 2011. Coactivators necessary for transcriptional output
- of the hypoxia inducible factor, HIF, are directly recruited by ARNT PAS-B. Proc Natl
- 603 Acad Sci U S A 108(19):7739-7744.
- 604 39. Collins, M. D., C. U. Kim, and S. M. Gruner. 2011. High-pressure protein
- crystallography and NMR to explore protein conformations. Annu Rev Biophys 40:81-
- 606 98.
- 40. Matthews, B. W. 2012. Proteins under pressure. Proc Natl Acad Sci U S A 109(18):6792-
- 608 6793.
- 609 41. Mozhaev, V. V., K. Heremans, J. Frank, P. Masson, and C. Balny. 1996. High pressure
- effects on protein structure and function. Proteins 24(1):81-91.
- 611 42. Rouget, J. B., T. Aksel, J. Roche, J. L. Saldana, A. E. Garcia, D. Barrick, and C. A.
- Royer. 2011. Size and sequence and the volume change of protein folding. J Am Chem
- 613 Soc 133(15):6020-6027.
- 614 43. Quinlan, R. J., and G. D. Reinhart. 2005. Baroresistant buffer mixtures for biochemical
- analyses. Anal Biochem 341(1):69-76.
- 44. Johnson, B. A. 2018. From Raw Data to Protein Backbone Chemical Shifts Using
- NMRFx Processing and NMRViewJ Analysis. Methods Mol Biol 1688:257-310.
- 618 45. Norris, M., B. Fetler, J. Marchant, and B. A. Johnson. 2016. NMRFx Processor: a cross-
- platform NMR data processing program. J Biomol NMR 65(3-4):205-216.
- 620 46. Elzhov, T. V. M., K. M.; Spiess, A.; Bolker, B. 2006. minpack.lm: R Interface to the
- Levenberg-Marquardt Nonlinear Least-Squares Algorithm Found in MINPACK, Plus
- 622 Support for Bounds. R package version 1.2-1. https://CRAN.R-
- project.org/package=minpack.lm.

- 624 47. Fossat, M. J., T. P. Dao, K. Jenkins, M. Dellarole, Y. Yang, S. A. McCallum, A. E.
- Garcia, D. Barrick, C. Roumestand, and C. A. Royer. 2016. High-Resolution Mapping of
- a Repeat Protein Folding Free Energy Landscape. Biophys J 111(11):2368-2376.
- 48. Turner, P. 2005. XMGRACE, Version 5.1. 19. Center for Coastal and Land-Margin
- Research, Oregon Graduate Institute of Science and Technology, Beaverton, OR.
- 629 49. Akasaka, K., H. Li, H. Yamada, R. Li, T. Thoresen, and C. K. Woodward. 1999. Pressure
- response of protein backbone structure. Pressure-induced amide 15N chemical shifts in
- 631 BPTI. Protein Sci 8(10):1946-1953.
- 50. Schrodinger, LLC. 2018. The PyMOL Molecular Graphics System, Version 2.1.
- 633 51. Chen, C. R., and G. I. Makhatadze. 2015. ProteinVolume: calculating molecular van der
- Waals and void volumes in proteins. BMC Bioinformatics 16:101.
- 52. Zwanzig, R. 1997. Two-state models of protein folding kinetics. Proc Natl Acad Sci U S
- 636 A 94(1):148-150.
- 637 53. Roche, J., J. A. Caro, D. R. Norberto, P. Barthe, C. Roumestand, J. L. Schlessman, A. E.
- Garcia, B. E. Garcia-Moreno, and C. A. Royer. 2012. Cavities determine the pressure
- unfolding of proteins. Proc Natl Acad Sci U S A 109(18):6945-6950.
- 640 54. Kharakoz, D. P. 1997. Partial volumes and compressibilities of extended polypeptide
- chains in aqueous solution: additivity scheme and implication of protein unfolding at
- normal and high pressure. Biochemistry 36(33):10276-10285.
- 643 55. Roche, J., C. A. Royer, and C. Roumestand. 2017. Monitoring protein folding through
- high pressure NMR spectroscopy. Prog Nucl Magn Reson Spectrosc 102-103:15-31.

- 645 56. Panick, G., G. J. Vidugiris, R. Malessa, G. Rapp, R. Winter, and C. A. Royer. 1999.
- Exploring the temperature-pressure phase diagram of staphylococcal nuclease.
- Biochemistry 38(13):4157-4164.
- 648 57. Font, J., A. Benito, R. Lange, M. Ribo, and M. Vilanova. 2006. The contribution of the
- residues from the main hydrophobic core of ribonuclease A to its pressure-folding
- 650 transition state. Protein Sci 15(5):1000-1009.
- 58. Zhang, S., Y. Zhang, N. E. Stenzoski, J. Zou, I. Peran, S. A. McCallum, D. P. Raleigh,
- and C. A. Royer. 2019. Pressure-Temperature Analysis of the Stability of the CTL9
- Domain Reveals Hidden Intermediates. Biophys J 116(3):445-453.
- 59. Zipp, A., and W. Kauzmann. 1973. Pressure denaturation of metmyoglobin.
- Biochemistry 12(21):4217-4228.
- 656 60. Royer, C. A. 2002. Revisiting volume changes in pressure-induced protein unfolding.
- 657 Biochim Biophys Acta 1595(1-2):201-209.
- 658 61. Beck Erlach, M., J. Koehler, B. Moeser, D. Horinek, W. Kremer, and H. R. Kalbitzer.
- 659 2014. Relationship between nonlinear pressure-induced chemical shift changes and
- thermodynamic parameters. J Phys Chem B 118(21):5681-5690.
- 661 62. Taulier, N., and T. V. Chalikian. 2002. Compressibility of protein transitions. Biochim
- Biophys Acta 1595(1-2):48-70.
- 663 63. Eneqvist, T., K. Andersson, A. Olofsson, E. Lundgren, and A. E. Sauer-Eriksson. 2000.
- The beta-slip: a novel concept in transthyretin amyloidosis. Mol Cell 6(5):1207-1218.
- 665 64. Panteva, M. T., R. Salari, M. Bhattacharjee, and L. T. Chong. 2011. Direct observations
- of shifts in the beta-sheet register of a protein-peptide complex using explicit solvent
- simulations. Biophys J 100(9):L50-52.